J Mater Sci (2019) 54:2122–2132

Composites

3D gel printing of graded TiC-high manganese steel cermet

Xinyue Zhang[1], Leichen Guo[2], Fang Yang[1,*], Alex A. Volinsky[3], Megan Hostetter[3], and Zhimeng Guo[1,*]

[1] Institute for Advanced Materials and Technology, University of Science and Technology Beijing, Beijing 100083, China
[2] School of Engineering Technology, Purdue University, West Lafayette, IN 47907, USA
[3] Department of Mechanical Engineering, University of South Florida, Tampa, FL 33620, USA

Received: 13 July 2018
Accepted: 20 September 2018
Published online: 26 September 2018

ABSTRACT

A new solid freeform process, 3D gel printing (3DGP), was proposed for designing and manufacturing graded composites. As an example, TiC-high manganese steel cermet with a gradient distribution of TiC was successfully designed and fabricated by 3DGP. The rheological behavior and polymerization of slurries with different TiC content have been researched. The complex-shaped green bodies were printed accurately by depositing slurries layer by layer. The scanning electron microscopy and X-ray diffraction revealed the gradient distribution and morphology of the TiC particles within a sintered sample. The density, hardness, abrasion wear resistance, transverse rupture strength and impact toughness of the 3D gel-printed TiC-high manganese steel cermet appeared graded distribution corresponding to its gradient structure. Gradient distribution of the composition, microstructure and mechanical properties of the 3D gel-printed part are consistent with the design concept. Results indicated that 3DGP is a promising approach for high-throughput design and fabrication of complex-shaped graded composites.

Introduction

Graded composites are a special class of composite materials, of which the composition and structure are designed to change gradually along certain pre-determined directions, resulting in a corresponding variation in the properties [1]. Many investigations have been conducted on the preparation and application of graded composites [2–4], indicating that the optimized design [5] enables composites to obtain optimal properties to meet varied performance requirements within a component. Currently, the greatest challenge is the gap between the traditional preparation processes and optimized design of graded composites.

In recent years, a series of technologies collectively called solid freeform fabrication (SFF), also known as additive manufacturing (AM), have attracted intensive interest because of their flexible manufacturing ability to translate the design concepts into 3D objects directly. Since all SFF technologies are based on the fundamental principle of layered manufacturing,

Address correspondence to E-mail: yangfang@ustb.edu.cn; zmguo@ustb.edu.cn

https://doi.org/10.1007/s10853-018-2945-5

there is substantial interest in applying SFF technologies to manufacture graded materials [6]. According to energy source for forming process, these SFF technologies can be divided into two classes: beam-based and non-beam-based technologies. Most of the existing investigations focus on beam-based technologies [7–9], which are based on using a laser or electron beam to selectively melt powder layer and bind it together to create a solid structure. However, there are some difficulties, such as residual thermal stresses, deformation, cracks and balling phenomena, which stem from the nature of beam-based technologies: rapid fusion and solidification at high temperature. Furthermore, beam-based processes are costly due to the laser/electron beam generator as well as protective device. In this situation, some researchers have turned to non-beam-based technologies, like fused deposition modeling (FDM) and three-dimensional printing (3DP). FDM is limited to polymer matrix composites [10]. 3DP is unable to manufacture fully dense components and is usually followed by pressure-less infiltration [11, 12], making the whole process complicated.

In order to put forward a high-throughput method for the design and production of graded metal matrix composites, a non-beam-based process, 3D gel printing (3DGP), is proposed in this paper. 3D gel printing is a stereo deposition technique based on deposition and in situ polymerization of slurry and shape formation by computer-controled slurry extrusion. Our previous studies on additive manufacturing of 316L stainless steel [13], ZrO_2 [14] and cemented carbide [15] have demonstrated general advantages of 3DGP, such as the flexibility in raw materials, simple structure of devices, forming ability of complex shapes, fine and uniform microstructure of the products.

The objective of this work is to explore the feasibility of using 3DGP in design and manufacturing of graded metal matrix composites. A steel-bonded carbide, TiC-high manganese steel cermet, was chosen as the raw material. The TiC-high manganese steel parts are mainly used for excavating, exploiting, drilling in the field of mining, oil and geology. High hardness and wear resistance of the stress-bearing surfaces and high toughness of the core region are required in parts subject to vibrations and impacts. The TiC-high manganese steel cermet is difficult to be machined because of its high hardness and work-hardening ability. Therefore, 3DGP was employed to obtain complex-shaped TiC-high manganese steel parts with a composition gradient.

Experimental procedure

3DGP process

As schematically depicted in Fig. 1a, the 3DGP procedure is composed of four steps: slurry preparation, design of 3D model and data processing, 3D gel printing, drying and sintering. A multi-syringe printer with layer-by-layer deposition function was used in this study. Figure 1b displays the deposition of slurry. The radical polymerization of organic monomer (HEMA in this study) took place and the deposited slurry solidified rapidly. Figure 1c is a schematic diagram for the printing process of the multi-syringe system. Under computer control, different slurries are extruded by different syringes and selectively deposited corresponding to 3D computer-aided design (CAD) database. By depositing slurries layer by layer, 3D parts are made.

Slurry preparation

The matrix material powders with a nominal composition of 14Mn-3Ni-2Mo-1.5C-79.5Fe (all in wt%) was mixed with various amounts of TiC powders (20, 30 and 40 wt%) by ball milling for 20 h, respectively. Carbonyl iron powder (99.5% purity, 3–5 μm), ferroalloys with Mn, Ni and Mo (99% purity, < 300 mesh) and graphite (99.5% purity, < 500 mesh) were used for making the high manganese steel matrix. The average particle size of TiC powder ($> 99.5\%$ purity) was 4 μm.

A non-aqueous gel system was chosen for preventing powder from oxidation: Hydroxyethyl methacrylate (HEMA), toluene and N, N′-methylene-bis-acrylamide (MBAM) were used as the organic monomer, solvent and crosslinker, respectively. HEMA and MBAM were dissolved in toluene to prepare a premixed solution. The prepared TiC-high manganese steel composite powders with different contents of TiC, 20 wt%, 30 wt% and 40 wt%, were added in the premixed solution. Three well-dispersed slurries with a solid loading of 60 vol% were prepared by planetary ball milling for 1 h.

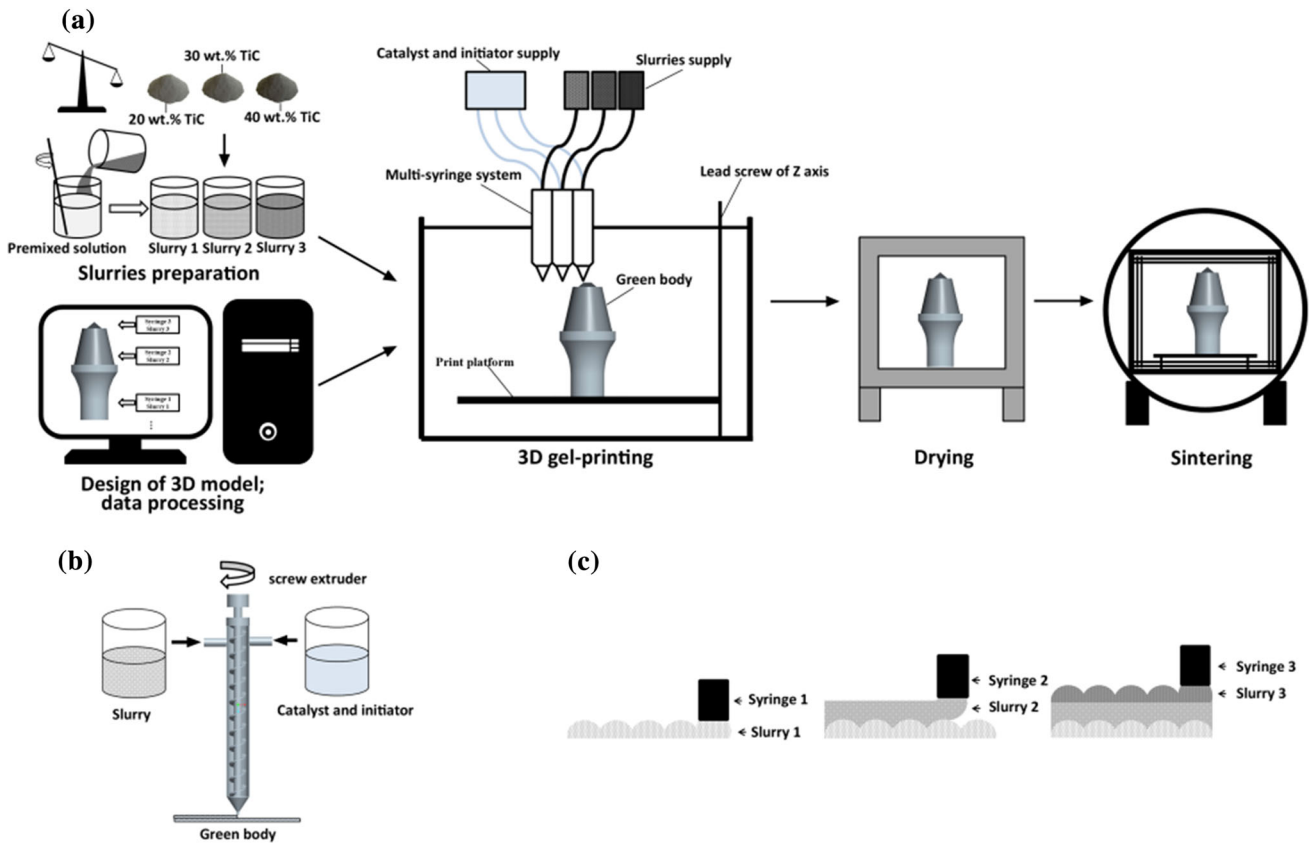

Figure 1 Schematic diagram of 3D gel printing: **a** steps in the 3DGP process for fabricating graded composites, **b** extrusion and deposition of slurry, **c** the principle of multi-syringe system for selectively depositing slurries.

Design of 3D model and data processing

A cutting pick (Fig. 5a) with a gradient distribution of TiC was designed in the 3D modeling software and then sliced into layers (layer height was 0.33 mm). The model data was further processed by 3D printing software to specify different syringes for depositing slurries at different locations within the cutting pick.

3D gel printing

After preliminary testing, the suitable printing parameters (0.4-mm needle of the syringes, 0.33 mm layer height, 23 mm/s extrusion speed of slurry, 20 mm/s printing speed) were adopted for this forming process. By depositing different slurries layer by layer, the cutting pick with a gradient distribution of TiC was printed. Meanwhile, several bulk samples were printed for microstructure and mechanical examinations.

Drying and sintering

After freeforming, samples were dried in a vacuum oven at 60 °C for 8 h. The dried green samples were debonded at 500 °C for 1 h with a heating rate of 3 °C/min in a vacuum carbon tube furnace (vacuum degree < 10 Pa). Then, the sintering process was carried out, as shown in Fig. 2, which consisted of four stages: 800 °C for 1 h, 1100 °C for 1 h, 1200 °C for 1 h and 1350 °C for 1 h. Subsequently, the sintered samples were performed furnace cooling to room temperature. Lastly, the sintered samples were solution treated at 1080 °C for 1 h and then water quenched.

Characterization

The rheological properties of the TiC-high manganese steel slurries were measured using a NDJ-79 rotary viscosity meter. The surface appearance and cross-sectional morphology of the 3DGP-built green bodies were observed by a confocal laser scanning

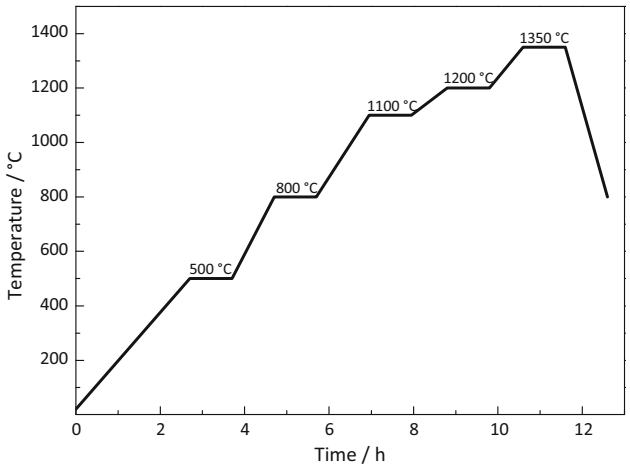

Figure 2 Debinding and sintering curve of 3D gel-printed sample.

microscope (CLSM, OLYPUS LEXT OLS4100). Thermal gravimetric analysis was applied to study the thermo-decomposition behaviors of toluene–HEMA gel at a heating rate of 10 °C/min under flowing high-purity argon atmosphere. The microstructures were investigated by scanning electron microscopy (SEM, LEO-1450). Phase composition was determined by X-ray diffraction on a TTR III diffractometer with Cu Kα radiation (λ = 0.1542 nm). The density of the sintered samples was determined by the Archimedes immersion method in water. Hardness test was carried out by a Rockwell hardness tester (HR-150A). The wear resistance was measured according to the standard procedure ASTM B611-13. The measurements were carried out using a wear tester (MLS-225) with 30 mesh aluminum oxide particles as the abrasive medium and a load of 200 N. The bars of 5 mm × 5 mm × 35 mm were cut from different regions of the quenched samples as specimens of transverse rupture strength tests which were performed on an Instron CMT 4305 electronic universal testing machine at a loading rate of 0.5 mm/min. The impact absorbed energy was measured at room temperature by Charpy test with 10 mm × 10 mm × 55 mm unnotched specimens. Each set of data reported was based on the properties obtained from five samples.

Results and discussion

There are several critical issues that need to be met before the 3DGP forming process. One key point is to produce homogeneous and flowable slurries with the highest possible solid loading value [16]. In this study, the toluene–HEMA gel system provided a low-viscosity vehicle and three well-dispersed slurries with a solid loading of 60 vol% and suitable viscosity, below 3 Pa·s at the shear rate of 20 s^{-1}, were prepared. As shown in Fig. 3a, the viscosity of three slurries decreased significantly with increasing shear rate, suggesting the shear thinning behavior. This behavior is conducive to the extrusion and deposition of slurries. The second challenge is the induction period of the slurry's polymerization. The deposition of slurries was based on free radical polymerization [17] of organic monomer. It can be seen from Fig. 3b that the induction period decreased with the increase in catalyst concentration, indicating that the polymerization of HEMA monomer can be controled by adjusting the concentration of catalyst *N*, *N*, *N*′, *N*′-tetramethylethylenediamine (TEMED). The third thing is the removal of polymeric gel inside the printed samples. The TG curve of toluene–HEMA polymeric gel (Fig. 3c) indicated that at a tempering temperature of 500 °C, a weight loss of almost 100% was recorded due to complete burn out of the polymeric gel.

The key parameters for a 3DGP process are the inner diameter of the needle, layer height, extrusion speed of slurry (slurry flowing speed inside the needle) and printing speed (movement speed of needle). After extruded, the shape of slurry filament changed due to the rheological property and weight of slurry. Figure 4a displays the basic condition of continuous printing: The volume of extruded slurry (V_{ext}) is equal to the volume of deposited slurry (V_{dep}), which would be calculated by using Eq. (1):

$$V_{ext} = V_{dep} \tag{1}$$

$$\frac{\pi}{4} D_n^2 \times v_{slu} \times t = A \times v_n \times t \tag{2}$$

$$\frac{\pi}{4} D_n^2 \times v_{slu} = A \times v_n \tag{3}$$

where D_n is the inner diameter of the needle, v_{slu} is the extrusion speed of slurry, v_n is the movement speed of needle, and A is the cross-sectional area of the slurry filament. The stacking manner of a slurry wall is depicted in Fig. 4b [18]. Based on this figure,

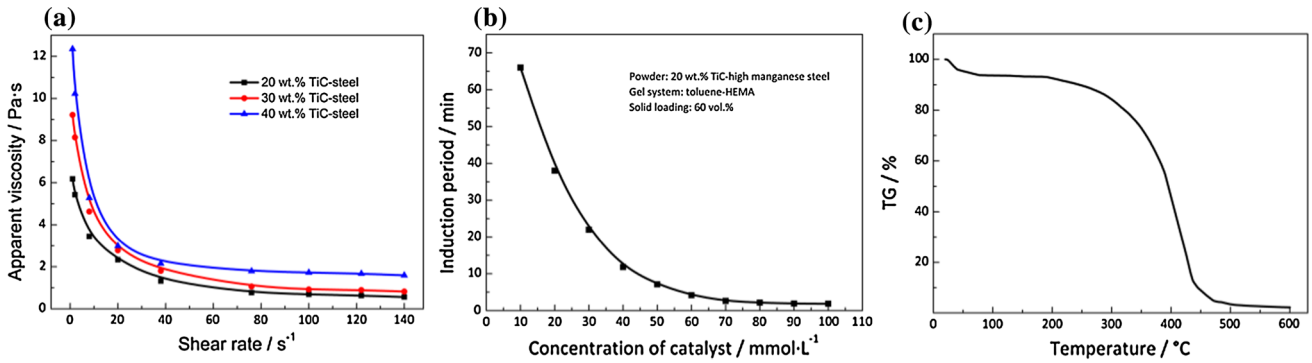

Figure 3 **a** Viscosity of the TiC-high manganese steel composite slurries as a function of shear rate, **b** Effect of catalyst concentration on the polymerization rate of 20 wt% TiC-high manganese steel composite slurry, **c** TG curve of polymeric gel with a heating rate of 10 °C/min.

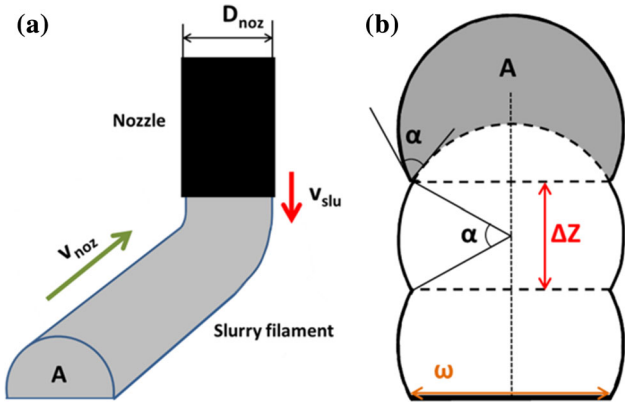

Figure 4 **a** Deformation of slurry filaments, **b** Cross-sectional illustration of a slurry wall.

the relationship between the layer height (Δz) and width of slurry filament (ω) can be concluded:

$$\Delta z = \omega \times \sin\frac{\alpha}{2} \tag{4}$$

where α is the slurry–green body contact angle. The cross-sectional area of the slurry filament A can be approximately calculated according to Eq. (5):

$$A = \omega \times \Delta z \tag{5}$$

By combining Eq. (3), (4) and (5), the layer height can be derived as:

$$\Delta z = \sqrt{\frac{\sin\frac{\alpha}{2} \times \pi \times D_n^2 \times v_{slu}}{4v_n}} \tag{6}$$

Equation (6) presents the implications of the key parameters of a good printing quality in 3DGP process. A green body with high precision and uniform microstructure could be achieved only if these key parameters arrive at a reasonable combination. Furthermore, it is generally agreed upon that the layer thickness and build orientation are the two major factors affecting the surface roughness of printed samples [19]. Our previous studies suggest that the print quality can be improved using a fine needle, thin layer and low printing speed. However, considering the print quality and efficiency, the suitable printing parameters (0.4-mm needle, 0.33 mm layer height, 23 mm/s extrusion speed of slurry, 20 mm/s printing speed) were adopted for this forming process.

Characterization of green body

Cutting pick with a gradient distribution of TiC was printed as an example, shown in Fig. 5b. The height and diameter of the model are 110 mm and 50 mm, respectively. The dimension of the printed cutting pick is 110.46 ± 0.02 mm high, 50.22 ± 0.02 mm in diameter. The shape and dimensions of the cutting pick are consistent with the designed 3D model. The printed lines can be observed with no defects on the surface. Note that the deposition angles of the cutting pick are well matched with the designed angles, as seen in Fig. 5c. More particularly, an overhang angle of about 60° was successfully printed without support material (Fig. 5d). The overhang angle, which is an important metric of formability of SFF process [20], is strongly related to the shear thinning behavior, shape retention and rapid polymerization of slurry. The maximum overhang angle (self-supporting angle) of 3DGP requires further exploration. Figure 5e shows a low magnification SEM image of the printed cutting pick's top surface. No gaps or defects exist between the compactly arranged printed

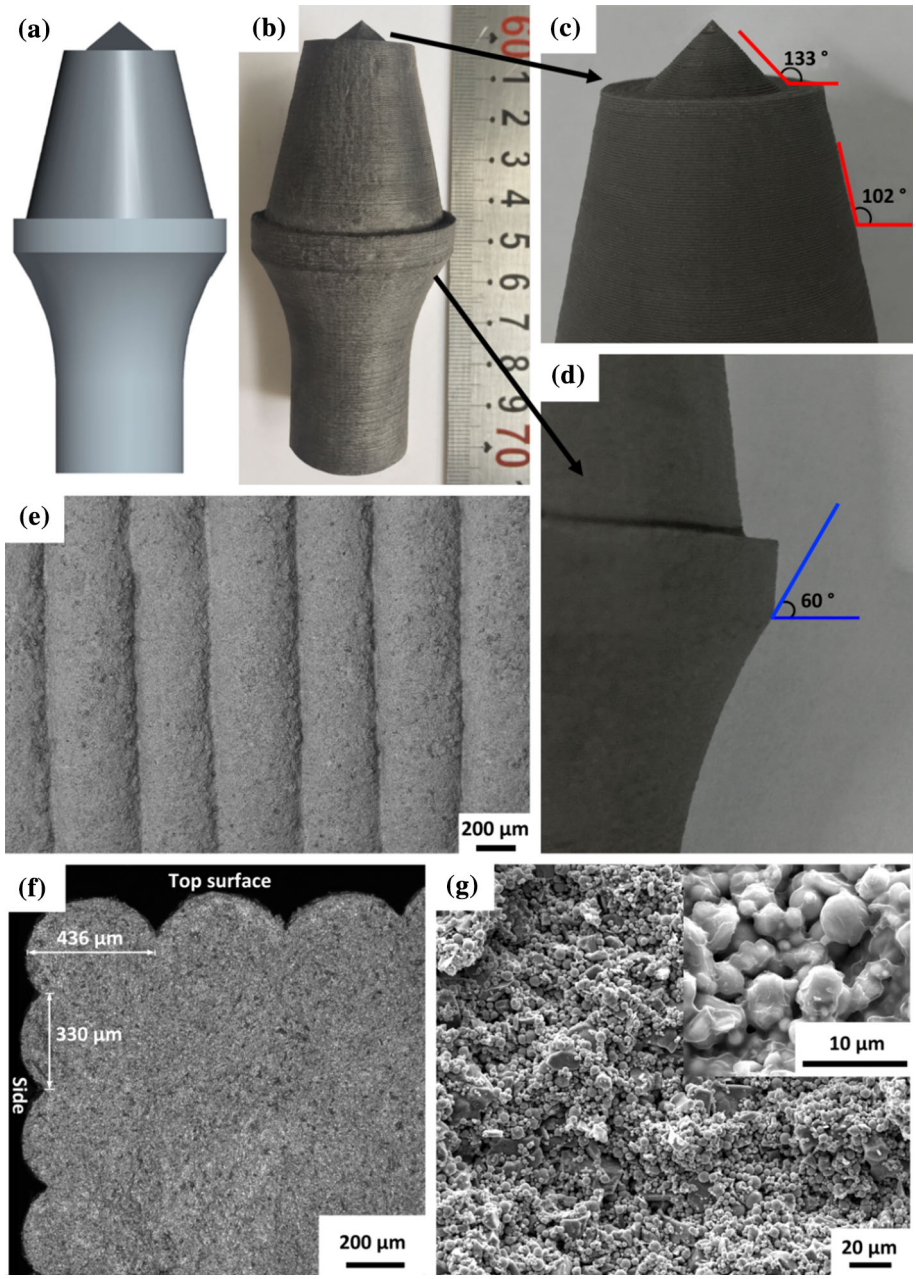

Figure 5 Characterization of 3DGP-built green bodies: **a** the designed cutting pick model with a gradient of TiC content, **b** 3DGP-built cutting pick, **c** the deposition angles and print accuracy of 3DGP, **d** an overhang angle of 60° without support material, **e** SEM image of the cutting pick's top surface, **f** fracture morphology of the 3DGP-built green body, **g** microstructure of dried green body.

lines. After being extruded and deposited on the print platform, the shape of the slurry filament changed from cylindrical to elliptic cylindrical because of its own gravity and rheological behavior. Figure 5f displays the fracture morphology of the printed bulk sample. The width of a printed line is about 436 µm, slightly larger than the internal diameter of the needle. The layer height is about 330 µm, which was the set layer height. This indicates that the deposited slurry filaments kept their elliptic cylinder shape and solidified quickly with adequate strength to support the weight of the subsequent layers. 3DGP exhibits a good formability and high forming precision for complex-shaped parts. Interestingly, no pores or gaps were observed in the green body, suggesting excellent adhesion between printed lines and layers. One reason is related to the stereo deposition method of 3DGP, in which the slurry filaments are cross piled and the next layer will fill the void spaces of the preceding layer, as shown in Figs. 1c and 5f. Another reason is that the polymerization of monomer and crosslinker would occur not

only within the printed lines, but also on the interfaces during printing and drying steps, resulting in the close combination of printed lines and layers. In addition, the green body has a homogeneous microstructure and a relatively high density due to the high solid loading of slurries, as shown in Fig. 5g. The highly crosslinked polymer–solvent gels cover and hold the powders tightly, while maintaining the green body's strength. The bending strength of dried green body is 12 ± 0.8 MPa, enabling the sample to be removed safely from the print platform.

The sintered samples

A representative cross-sectional (parallel to deposition direction) microstructure of the sintered bulk sample is shown in Fig. 6a. The SEM image shows the gradient distribution of TiC (the dark gray particles in the image) within the TiC-high manganese steel composite. The gradient structure of 3D gel-printed sample was not destroyed by sintering at high temperature. The sintered 3DGP sample exhibited a clear graded distribution of TiC, which was consistent with the design concept. Moreover, no defects or interfaces between the printed layers and lines were observed. The sample with nearly full densification consisted of three deposition regions corresponding to three slurries with TiC content of 20 wt%, 30 wt% and 40 wt%. The micrographs of the three deposition regions, Fig. 6b–d, demonstrate the distribution of TiC particles and dissolution–reprecipitation reaction of TiC particles in the binder phase. It should be noted that the Mo element in high manganese steel matrix would produce TiC–Mo_2C phase which surrounds the TiC particles, presenting a core–shell structure in the microstructure. There are obvious core–shell structures in Fig. 6b–d, which are contributed to the wetting between reinforcement particles and metal matrix. The microstructure of the sintered 3DGP sample is similar to that of specimens made by powder metallurgy.

XRD investigations were performed on three deposition regions mentioned above inside a 3DGP sample. It is observed in Fig. 7 that only the diffraction peaks corresponding to TiC and austenite matrix are present without any significant contamination. After water toughening, high manganese steel matrix is single-phase austenite. The relative intensity of the TiC peak gradually increased from region 1 to region 2 to region 3, indicating the TiC content increased. XRD patterns also verified the gradient distribution of TiC in the TiC-high manganese steel composite.

The density and mechanical properties of 3DGP sample also showed graded distribution. To evaluate the density and hardness, several cubes (10 mm × 10 mm × 10 mm) were cut from different regions in the sintered samples. The sintered density decreased with the TiC content, providing a 6.79–6.5–6.22 $g{\cdot}cm^{-3}$ gradient. The theoretical density of graded TiC-high manganese steel composite (20 wt%–30 wt%–40 wt%) is 6.8–6.5–6.22 $g{\cdot}cm^{-3}$. The fully densified TiC-high manganese steel cermet with a gradient distribution of TiC was obtained. Hardness values along the TiC-high manganese steel cermet increased with the content of TiC, revealing a gradient of 45.6–52.8–59.9 HRC (Fig. 8).

The specimens for high-stress abrasive wear tests were cut from three regions of 3DGP samples as well. The specimens were held in a vertical position tangent to a rotating steel wheel immersed in water slurry of aluminum oxide particles. The test duration was 10 min (1000 revolutions at 100 rpm). In this study, the weight loss has been converted to volume loss due to the different densities of specimens. The wear resistance was evaluated by volume loss: the lower the volume loss, the better the wear resistance. The results are shown in Fig. 8. It has been observed that the volume loss is more in the case of the specimen with 20 wt% TiC content. The specimens cut from region 3 (40 wt% TiC) achieved the minimal volume loss, exhibiting the best wear resistance. It is well known that high manganese steel has a work-hardening capacity and an excellent wear resistance under high-stress abrasive wear condition. And the addition of TiC particulate reinforcements could significantly improve the wear resistance of the high manganese steel matrix. The volume loss decreased with the increasing TiC content because plowing and cutting of the matrix by the abrasive particles were reduced by the presence of the hard TiC particles. The wear resistance of 3DGP samples showed a gradient variation (volume loss gradient: 0.034–0.009–0.007 cm^3) according to their composition gradient and microstructure gradient.

Figure 9a shows the transverse rupture strength (TRS) and impact toughness values of 3DGP samples. A significant drop in the TRS and impact toughness has been observed from region 1 to region 3. In addition, it can be seen from Fig. 9b that the TRS values decrease considerably with the increase of TiC content.

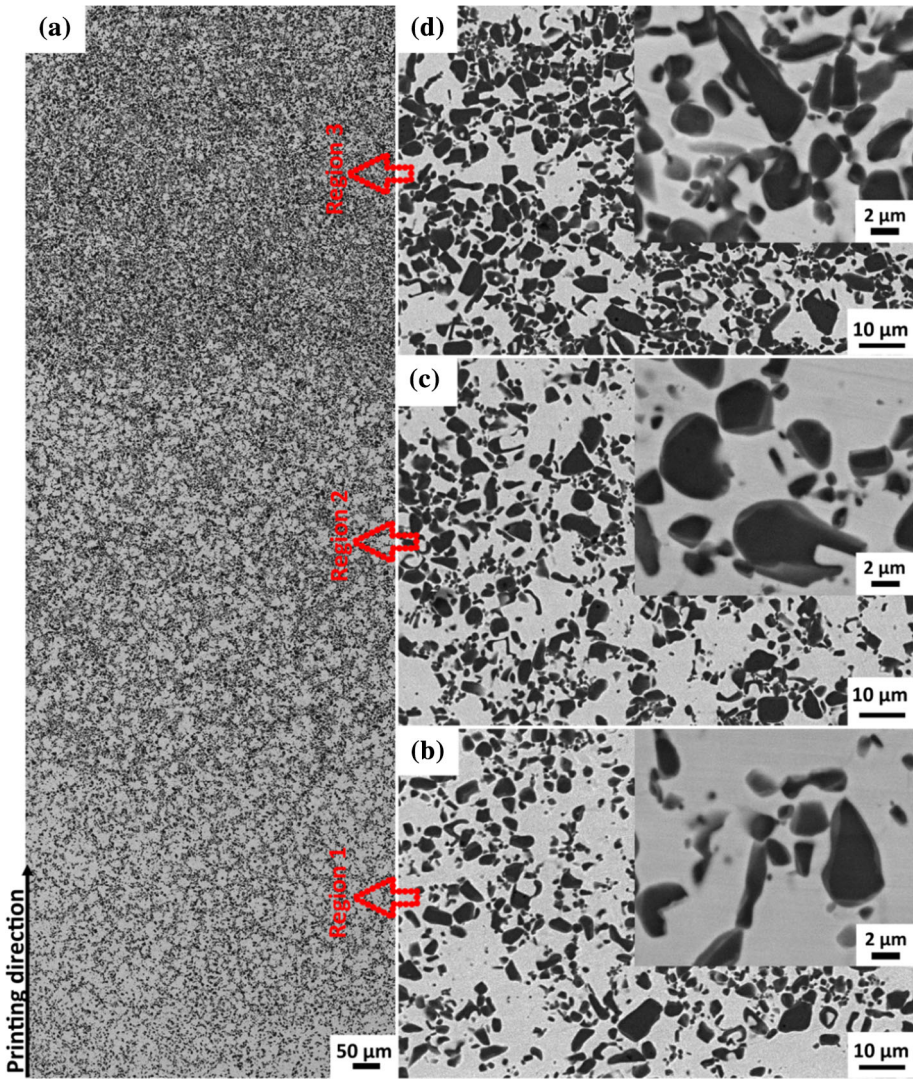

Figure 6 **a** Typical longitudinal section microstructure of the sintered, compositionally graded TiC-high manganese steel composite, SEM images with **b** 20 wt% TiC, **c** 30 wt% TiC and **d** 40 wt% TiC content.

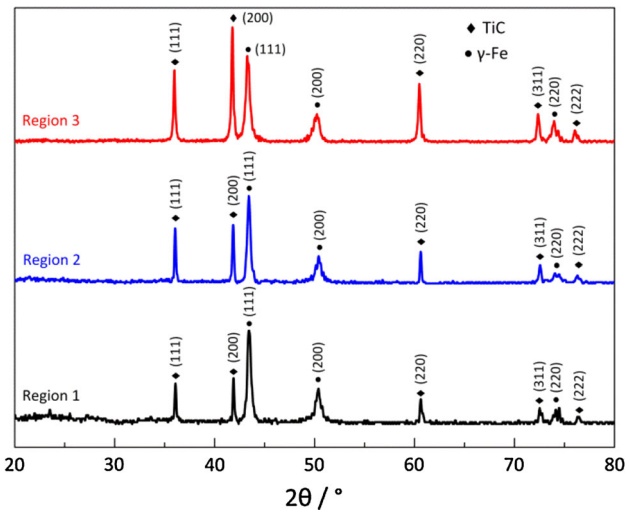

Figure 7 XRD patterns of three regions of 3D gel-printed TiC-high manganese steel composite.

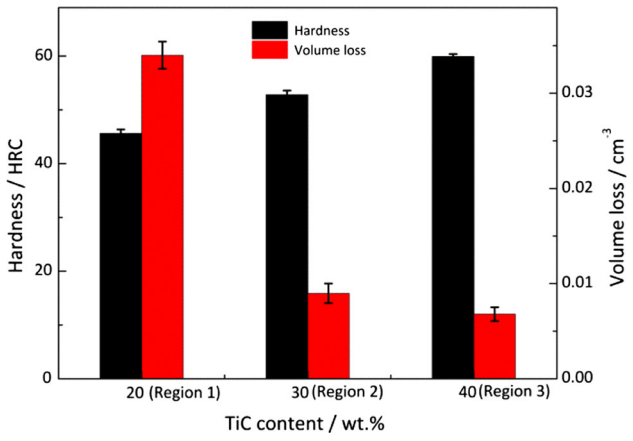

Figure 8 Gradient variations of hardness and wear resistance of 3D gel-printed graded composite.

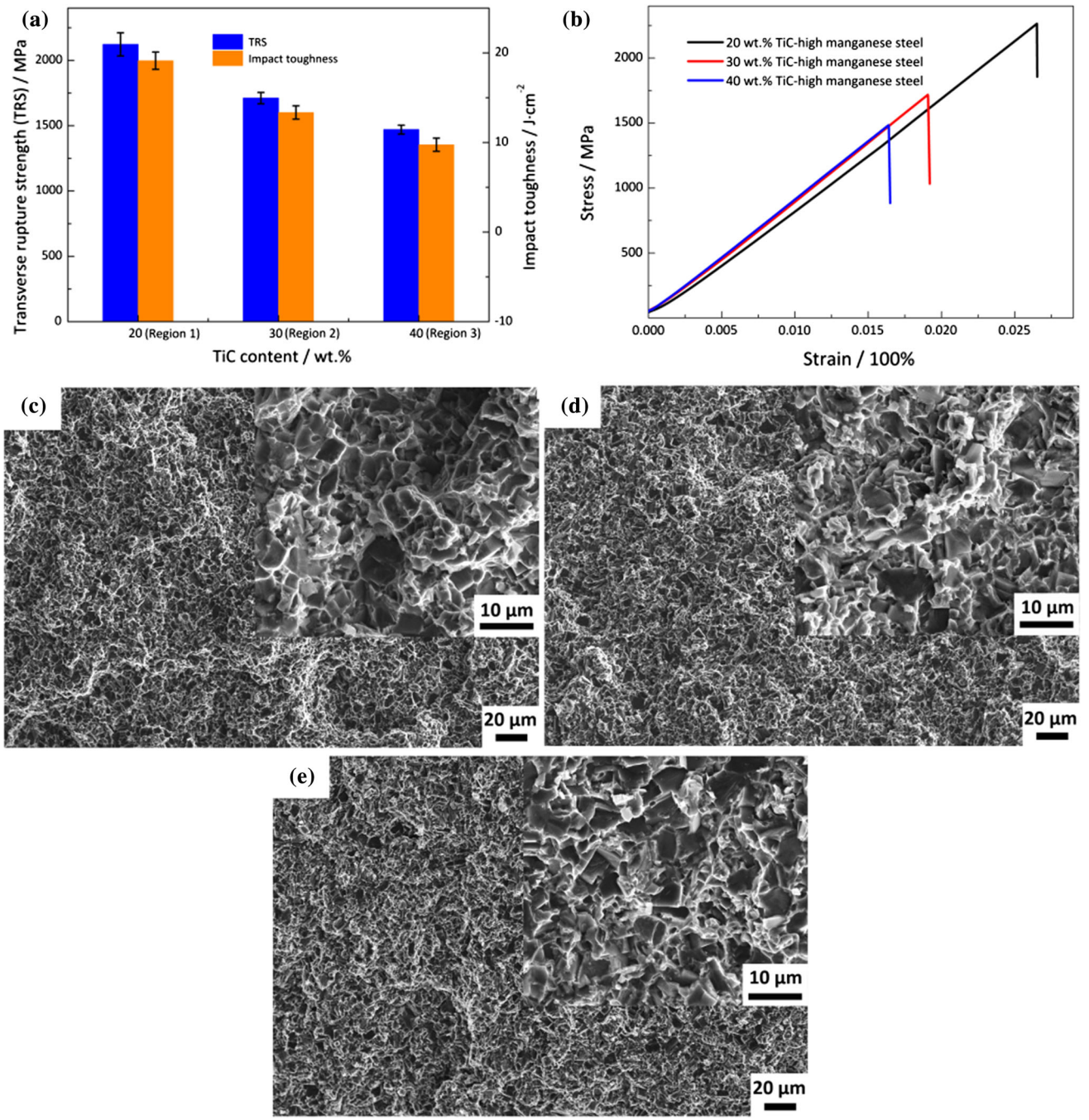

Figure 9 **a** Transverse rupture strength and impact toughness of graded TiC-high manganese steel composite, **b** stress–strain curves of graded samples, fracture morphology of specimens with **c** 20 wt% TiC, **d** 30 wt% TiC and **e** 40 wt% TiC.

The increase in TiC content from 20 to 40 wt% led to a decrease in the toughness and deformation capability of the composite materials. The TRS and impact toughness gradient were 2122.7–1711.3–1470.3 MPa and 19.14–13.35–9.75 J·cm^{-2}, respectively. The SEM micrographs of fractured surface of 3DGP samples were shown in Fig. 9c–e. The fractured surface of low TiC content specimen (20 wt%) shows the brittle fracture of TiC particles mixed with a certain amount of the ductile fracture of high manganese steel matrix. With increasing TiC content, the ductile fracture of matrix decreased remarkably, whereas the brittle fracture of TiC particles became the dominant fracture feature. It is difficult to see the ductile fracture of matrix on the

fractured surface of the specimen with 40 wt% TiC. The fracture appearance also suggests that the TRS and impact toughness of 3DGP sample decrease with increasing TiC content, appearing graded distribution.

In this article, a cutting pick with gradient TiC structure and corresponding graded mechanical properties was designed and fabricated rapidly by 3D gel printing. As a non-beam-based process, 3DGP avoids the problems caused by high-energy, high-temperature and rapid solidification and has the capabilities to manufacture fully dense complex-shaped graded parts. It is worth pointing out that 3DGP is a high-throughput design and manufacturing method. This method opens the gate for integration between design and manufacturing of graded composites. Nevertheless, further research needs to be invested on 3DGP for the optimal design and additive manufacturing of more graded composites and more complex-shaped parts.

Conclusions

A non-beam-based SFF technique termed 3D gel printing was successfully employed to design and manufacture TiC-high manganese steel composites with a gradient distribution of TiC. Three slurries with different TiC content were prepared based on toluene–HEMA gel system, of which rheological behavior was appropriate for 3DGP process. The complex-shaped green bodies were printed accurately by depositing different slurries layer by layer. After sintering, the manufactured cutting pick and samples had gradient structure with corresponding graded mechanical properties. The corresponding density, hardness, TRS and impact toughness gradient were 6.79–6.5–6.22 g cm^{-3}, 45.6–52.8–59.9 HRC, 2122.7–1711.3–1470.3 MPa and 19.14–13.35–9.75 J cm^{-2}, respectively. The wear resistance increased considerably by the increase in TiC content within a 3DGP sample. The cutting pick with high hardness and excellent wear resistance of the stress-bearing tip and surface and high toughness of the tail completely conformed to the design concept. In addition, this study proves that fully dense complex-shaped part with a gradient distribution of reinforcing particles (TiC in this study) and properties can be fabricated. 3DGP has shown distinctive advantages and capabilities for the integrated design and manufacturing of graded composites over traditional manufacturing processes and other SFF techniques, providing a new high-throughput method of producing graded composite parts with desired properties gradient.

Acknowledgements

This work was supported by the Fundamental Research Funds for the Central Universities (No. FRF-TP-16-017A1) and the State Key Lab of Advanced Metals and Materials (No. 2016-ZD02).

Compliance with ethical standards

Conflict of interest The authors claim no conflicts of interest.

References

[1] Hui PM, Zhang X, Markworth AJ, Stroud D (1999) Thermal conductivity of graded composites: numerical simulations and an effective medium approximation. J Mater Sci 34:5497–5503. https://doi.org/10.1023/A:1004760427981

[2] Put S, Anné G, Vleugels J, Van der Biest O (2004) Advanced symmetrically graded ceramic and ceramic-metal composites. J Mater Sci 39:881–888. https://doi.org/10.1023/B:JMSC.0000012917.51982.9d

[3] Simchi A, Rota A, Imgrund P (2006) An investigation on the sintering behavior of 316L and 17-4PH stainless steel powders for graded composites. Mater Sci Eng, A 424:282–289

[4] Firouzdor V, Simchi A, Kokabi AH (2008) An investigation of the densification and microstructural evolution of M2/316L stepwise graded composite during co-sintering. J Mater Sci 43:55–63. https://doi.org/10.1007/s10853-007-2077-9

[5] Markworth AJ, Ramesh KS, Parks WP Jr (1995) Modelling studies applied to functionally graded materials. J Mater Sci 30:2183–2193. https://doi.org/10.1007/BF01184560

[6] Tammas-Williams S, Todd I (2017) Design for additive manufacturing with site-specific properties in metals and alloys. Scripta Mater 135:105–110

[7] Chung H, Das S (2006) Processing and properties of glass bead particulate-filled functionally graded Nylon-11 composites produced by selective laser sintering. Mater Sci Eng, A 437:226–234

[8] Balla VK, DeVasConCellos PD, Xue W, Bose S, Bandyopadhyay A (2009) Fabrication of compositionally and structurally graded Ti–TiO_2 structures using laser engineered net shaping (LENS). Acta Biomater 5:1831–1837

[9] Tan X, Kok Y, Tan YJ, Descoins M, Mangelinck D, Tor SB, Leong KF, Chua CK (2015) Graded microstructure and

mechanical properties of additive manufactured Ti–6Al–4 V via electron beam melting. Acta Mater 97:1–16

[10] Zhong W, Li F, Zhang Z, Song L, Li Z (2001) Short fiber reinforced composites for fused deposition modeling. Mater Sci Eng, A 301:125–130

[11] Levy A, Miriyev A, Elliott A, Babu SS, Frage N (2017) Additive manufacturing of complex-shaped graded TiC/steel composites. Mater Des 118:198–203

[12] Moon J, Caballero AC, Hozer L, Chiang Y, Cima MJ (2001) Fabrication of functionally graded reaction infiltrated SiC–Si composite by three-dimensional printing (3DP^{TM}) process. Mater Sci Eng, A 298:110–119

[13] Ren X, Shao H, Lin T, Zheng H (2016) 3D gel-printing: an additive manufacturing method for producing complex shape parts. Mater Des 101:80–87

[14] Shao H, Zhao D, Lin T, He J, Wu J (2017) 3D gel-printing of zirconia ceramic parts. Ceram Int 43:13938–13942

[15] Zhang X, Guo Z, Chen C, Yang W (2018) Additive manufacturing of WC-20Co components by 3D gel-printing. Int J Refract Met Hard Mater 70:215–223

[16] Young AC, Omatete OO, Janney MA, Menchhofer PA (1991) Gelcasting of alumina. J Am Ceram Soc 74(3):612–618

[17] Omatete OO, Janney MA, Nunn DS (1997) Gelcasting: from laboratory development toward industrial production. J Eur Ceram Soc 17:407–413

[18] Bryant FD, Sui G, Leu MC (2003) A study on effects of process parameters in rapid freeze prototyping. Rapid Prototyping J 9(1):19–23

[19] Lalehpour A, Barari A (2018) A more accurate analytical formulation of surface roughness in layer-based additive manufacturing to enhance the product's precision. Int J Adv Manuf Technol 96:3793–3804

[20] Yu HZ, Jones ME, Brady GW, Griffiths RJ, Garcia D, Rauch HA, Cox CD, Hardwick N (2018) Non-beam-based metal additive manufacturing enabled by additive friction stir deposition. Scripta Mater 153:122–131